

Research Article

Identification of potential human chymase inhibitors using molecular docking and molecular dynamics simulation

Asiya Rozindar

Department of Biotechnology, Basaveshwar Engineering College, Bagalkot- 587102 (Karnataka) India

Virupakshaiah DBM*

Department of Microbiology Shivagangotri Davangere University, Davangere -577007 (Karnataka), India

Bharati S. Meti

Department of Biotechnology Basaveshwar Engineering College, Bagalkot-587102 (Karnataka), India

Bजारंग Vasant Kumbha

Department of Biological Sciences, Sunandan Divatia School of Science, NMIMS University Vile Parle (West), Mumbai- 400056 (Maharashtra), India

Ajay Kumar Oli

Department of Biomedical Science, SDM Research Institute for Biomedical Sciences, Shri Dharmasthala Manjunatheshwara University, Sattur- Dharwad - 580009 (Karnataka), India

*Corresponding author. E mail: virudbm@gmail.com

Article Info

<https://doi.org/10.31018/jans.v15i1.3324>

Received: February 22, 2022

Revised: January 5, 2023

Accepted: January 8, 2023

How to Cite

Rozindar, A. *et al.* (2023). Identification of potential human chymase inhibitors using molecular docking and molecular dynamics simulation. *Journal of Applied and Natural Science*, 15(1), 1 - 8. <https://doi.org/10.31018/jans.v15i1.3324>

Abstract

Chymase is a hydrolase class of enzymes that involves hydrolysis of peptide bonds. It is abundant in secretory granules of mast cells. Mast cell chymase is involved in the synthesis of angiotensin-II from its precursor protein. In addition, chymase is involved in converting TGF- β and matrix metalloproteinase to their active form. Chymase involved in heart failure has been proven, and its inhibition may reduce the progression. Hence, to identify the potential inhibitors against the chymase, the present study employed structure-based virtual screening, molecular docking, and molecular dynamics simulation to identify potential chymase inhibitors. Initially, compounds were selected based on their physicochemical and pharmacokinetic properties. Further, the binding affinities using molecular docking and interaction analyses were performed to find potential chymase inhibitors. The study identified chymase inhibitor ZINC000008382327, bearing significant binding affinity, specificity, and efficacy towards the chymase. Next, the stability and binding mode of chymase with ZINC000008382327 were assessed using molecular dynamics simulations. The simulation analysis using root mean square deviations and fluctuations revealed that inhibitor ZINC000008382327 affected the structure and dynamics of the chymase protein. It was also shown that the chymase forms a stable complex with ZINC000008382327 during the simulation. Thus, the present computational study put forward that the identified compound can be further exploited as a potential chemical scaffold to design and develop new human chymase inhibitors.

Keywords: ADMET, Docking, Mast cell chymase, Molecular dynamics simulation

INTRODUCTION

Chymase enzyme inhibition roles for the treatment modality for heart failure, asthma, and type of hypersensitive reaction related to mast cell degranulation (Doggrell and Wanstall 2004; Caughey, 2016). Chymase catalyzes the hydrolysis of peptide bonds and it is stored in the secretory granules of mast cells (Doggrell and Wanstall 2004). On the release, chymase remains

bound to the extracellular matrix and is functional for some weeks (Pejler, 2020). Chymase hydrolysis the substrate like angiotensin I to angiotensin II which is involved in vascular remodeling (Miyazaki and Takai 2001; Doggrell and Wanstall, 2004). It also induces the apoptosis of smooth muscle cells by degrading the fibronectin (Leskinen *et al.*, 2003). It also degrades the extracellular matrix through the activation of matrix metalloprotease I and III as well as transforming growth

factor- β (TGF- β) (Tchougounova *et al.*, 2005; Lundquist *et al.*, 2006).

Earlier, potential chymase inhibitors such as chymostatin show incompatible with *In-vivo* studies (Roszkowska-Chojecka *et al.*, 2015). Initially, Suc-Val-Pro-Phe^P(OPh)₂ was used as a potential inhibitor for chymase (Zhang *et al.*, 2016). Subsequently, orally active chymase inhibitors have been developed including BCEAB and SUN-C8257, with IC₅₀ values of 5.4 nM and 0.31 μ M, respectively (Takai *et al.*, 2003). In addition, the ASB17061 inhibitor prevented the development of angiotensin II-induced abdominal aortic aneurysm in apolipoprotein E-deficient mice (Tomimori *et al.*, 2019). Besides, SF2809 compounds from *Dactylosporangium* sp. were reported as chymase inhibitors (Tani *et al.*, 2004). In the present study, physicochemical and pharmacokinetic properties of chymase inhibitors, along with molecular and molecular dynamics simulation, were performed to determine a potential molecule for inhibitions of chymase.

MATERIALS AND METHODS

Protein modeling, inhibitor library preparation, and computational tools

The three-dimensional atomic coordinates of mast cell chymase protein were retrieved from the protein database with source code 3N7O.PDB (Kervinen *et al.*, 2010). The non-standard molecules e.g. H₂O and N₇O inhibitors, were removed from the crystal structure. Next, the mast cell chymase protein structure was prepared for virtual high throughput screening by adding H atoms to the polar atoms, followed by assigning appropriate atom types. The mast cell chymase inhibitors were retrieved from the ZINC database. To identify the potential drug candidate using various computational structural biology software including the AutoDock Tools (Morris *et al.*, 2009), AutoDock Vina (Trott and Olson 2010) for drug screening, GROMACS 2020.1 for molecular dynamics simulation (VanDer *et al.*, 2005). Besides, PyMol (DeLano 2002) and Discovery Studio Visualizer (BIOVIA 2016) were used for the data visualization and analysis. The visualization of MD trajectories Visual Molecular Dynamics (VMD) software (Humphrey *et al.*, 1996) was used. Along with this, the data retrieval, evaluation, and analysis of the Protein Data Bank, ZINC database (Sterling and Irwin 2015), and Swiss ADME server (Daina *et al.*, 2017) were used.

Physicochemical and drug-likeness properties

The mast cell chymase inhibitors collected from the ZINC library were screened out based on their physicochemical and ADME-T properties using Swiss ADME (Daina *et al.*, 2017). We have selected compounds satisfying Lipinski's rules of five (Barret 2018). Next, we applied Pan-assay interference compounds (PAINS) to

screen compounds with a higher affinity to bind toward multiple target receptors. Here, compounds possessing excellent ADME-T and PAINS properties were further selected for docking studies.

Molecular docking study

Molecular docking was performed to screen the compounds based on their binding affinities towards mast cell chymase using the AutoDock Vina (Trott and Olson 2010) software. Earlier, the inhibitor binding region of chymase was identified and which consists of residues Lys40, His57, Tyr94, Asn95, Thr96, Leu99, Asp102, Ala190, Phenylalanine191, Lys192, Gly193, Ser195, Val213, Ser214, Tyr215, Gly216, and Arg217 (Arooj *et al.*, 2013). The human chymase crystal structure used in the study is co-crystallized with the inhibitor N₇O (Arooj *et al.*, 2013). Hence, in this study, the grid box was set around this site with a search space of 40 \times 40 \times 40 \AA , centralized at X-axis -9.494, Y-axis -48.641, and Z-axis -58.495, respectively. The grid spacing was set to 0.375 \AA with default docking parameters. Each compound's least binding energy conformation was visualized and analyzed using the PyMOL software (DeLano 2002). The 2D interaction of inhibitors with human chymase was analyzed using the Discovery studio visualization (Biovia 2016). Here, we have selected only two compounds that have the least energy and more interacting residues with binding site pocket amino acids of mast cell chymase protein, similar to N₇O inhibitors (Kervinen *et al.*, 2010).

Molecular dynamics simulation

The all-atom molecular dynamics simulation was performed on three systems which include mast cell chymase and mast cell chymase with ZINC000008382327 inhibitor using Amber-FF99SB force field through the GROMACS 2020.1 (VanDer *et al.*, 2005). Force field parameters for the drug inhibitor were generated using the GAFF through the 'Antechamber' module of AMBER18 (Case *et al.*, 2012). Further, the 'Xleap' module of 'AMBER Tools' was used to generate the topology and coordinates files. The MD simulation systems were solvated using a cubic water box with a TIP3P water type and added an equivalent number of counter-ions to neutralize the MD simulation system. These topology and coordinate files generated using the amber tools were changed to the GROMACS-friendly format, similar to earlier work on protein-drug complex (Kumbhar *et al.*, 2016, 2020). Next, energy minimizations were performed using the steepest descent followed by the conjugate gradient method. The equilibration MD simulation was performed using the NVT ensemble for 500 ps and the ensemble for 500 ps. The production simulation was performed for 20 ns for all the systems. The MD simulation trajectory was analyzed using the Xmgrace (Turner 2005), PyMOI (Warnecke *et al.*,

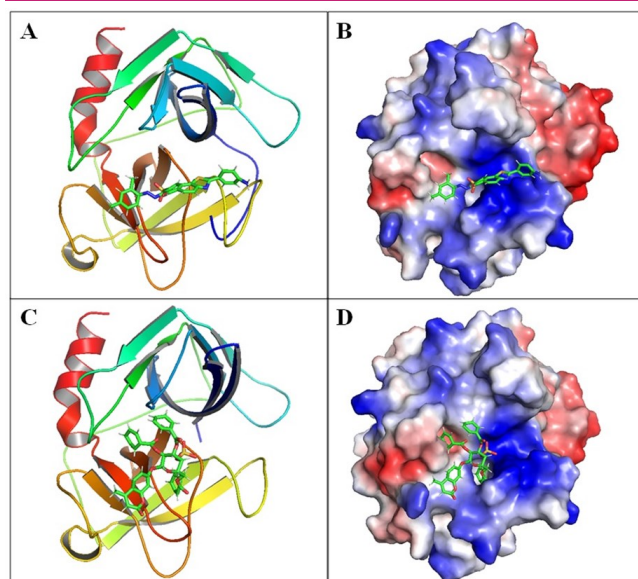


Fig. 1. Molecular docking of chymase with inhibitors, **A)** Showing chymase with ZN000003848531 inhibitor complex; **B)** Showing electrostatic potential surface of chymase with ZN000003848531 inhibitor binding pocket; **C)** Showing chymase with ZN000008382327 inhibitor complex, and **D)** Showing the electrostatic potential surface of chymase with ZN000008382327 inhibitor binding pocket.

2014), and Discovery Studio Visualizer (BIOVIA 2016). MD simulation trajectory movies were produced using the VMD, similar to an earlier study (Kumbhar and Bhandre, 2021).

RESULTS AND DISCUSSION

Physicochemical and ADMET properties

In the present study, the physicochemical properties revealed that three compounds fulfilled Lipinski's rule of five accepted properties of chymase inhibitor N₇O as shown in Table 1. Further, based on their Adsorption distribution metabolism tests, the excretion and toxicology (ADME-T) properties of the selected and standard N₇O inhibitors are listed in Table 2. The biological activity of chymase inhibitors against compounds is shown in Table 3.

Docking of chymase with inhibitors

Molecular docking of chymase with inhibitors, the two compounds showed ZN000008382327 and ZN000003848531 significant binding energy of -9.4 kcal/mol and -10.0 kcal/mol, respectively with the mast chymase as shown in Fig. 1. The detailed analysis of hydrogen bonding, van der Waals, alkyl type, and pi-pi type of interactions was performed using the PyMol (DeLano 2002) and Discovery Studio Visualizer (BIOVIA, 2016). The docked complex of mast chymase with ZN000008382327 (Fig. 1A) shows bonding interactions with residues Lys28 (2.5 Å), His45 (2.6 Å), and Ser182 (2.1 Å), Gly199 (3.0 Å), and Ser192 (2.7 Å) shown in Table 4. Next, the docked complex of mast chymase with ZN000003848531 (Fig. 1C) shows the hydrogen bonding interactions with residues such as

Table 1. List of the chymase inhibitors with their physicochemical properties

S. No.	Compound ID	Mol. wt. (g/mol)	Rotatable bond	H bond acceptor	H-bond donor	Log P	Lipinski violation
1	ZINC000000058111	162.14	0	3	1	1.44	0
2	ZINC000000391177	176.17	1	3	0	2.06	0
3	ZINC000000967579	136.23	0	0	0	2.63	1
4	ZINC000000967580	136.23	0	0	0	2.36	1
5	ZINC000000968461	222.37	4	1	1	3.45	0
6	ZINC000000968466	184.28	1	0	0	2.93	1
7	ZINC000001632794	386.35	9	8	2	1.96	0
8	ZINC0000018497591	222.37	4	1	1	3.61	0
9	ZINC000003848531	504.58	4	7	3	2.81	1
10	ZINC000004029365	333.32	8	5	3	0.53	0
11	ZINC000004098143	306.35	2	5	1	2.12	0
12	ZINC000004416136	465.46	6	10	4	-0.20	1
13	ZINC000005883734	163.22	3	2	1	1.76	0
14	ZINC000006483403	332.26	2	8	5	2.02	0
15	ZINC000008382327	730.69	14	14	1	3.93	0
16	ZINC000009087678	424.41	9	7	4	1.15	0
17	ZINC000012888204	420.42	7	5	4	1.84	0
18	ZINC000022061412	424.41	5	8	4	0.07	0
19	ZINC000062233804	204.35	6	0	0	3.87	1
20	ZINC000068572312	364.43	6	4	1	2.18	0
21	ZINC000104370385	346.42	3	5	1	3.01	0
22	ZINC000169300751	346.42	3	5	1	3.01	0
23	Standard drug: N ₇ O	441.82	6	5	2	2.40	0

Gly180 (3.4 Å) and Tyr198 (2.8 Å) shown in Table 4. In addition, the inhibitors' bonding interactions showed the van der Waals, pi-pi, and pi-alkyl type of interactions with the chymase protein, as shown in Fig. 2.

PASS biological activity prediction

The biological activity of screened compounds using the PASS analysis shows that they possessed biological activities. The standard N70 inhibitor showed inhibitory action, validating the results predicted from the PASS server (Lagunin *et al.*, 2000). The compounds ZN000003848531 and ZN000008382327 have also shown biological activity for antibacterial, anti-infective, anti-fungal, and Lactase inhibitor activity, with Pa ranging from 0,325 to 0,799, when Pa > Pi.

Molecular dynamics simulation

The present study on simulation revealed the protein structural deviations, fluctuations, and dynamics during the simulation, C α backbone root means square deviation (RMSD) and fluctuation (RMSF) have been utilized and shown in Figs. 5-6. The structural stability of the chymase and chymase with ZN000008382327 complex based on the calculation using the RMSD of C α backbone atoms with time evolution, observed average values as 0.10 nm and 0.15 nm. The RMSD plot shows that the free form of chymase and chymase with ZN000008382327 complex is stable throughout the MD

simulation shown in Fig. 3. Free State chymase protein is stable during the simulation after the 5ns up to 20ns time steps. However, chymase with ZN000008382327 complex shows a higher RMSD value in comparison with free-state chymase Fig. 1.

Molecular Dynamics simulation showed that the ZN000008382327 formed a stable complex with chymase throughout the simulation, as shown in Fig.1. It also showed the chymase stable with another compound ZN000008382327. Further, to investigate the effect of ZN000008382327 inhibitor binding to the residual fluctuations of active site region of chymase in comparison with free form chymase, the C α backbone atoms RMSF plot was calculated and shown in Fig.4. The region 60-80, 115-131, 157-172, to 175 is mainly involved in the active site region and the fluctuations were found to be restricted and minimized upon binding of ZN000008382327 inhibitor. The RMSD plot reveals that the binding of the ZN000008382327 affects the conformational state of the chymase receptor, as shown in Fig. 4.

Next, to explore the conformational stability of the free form of mast chymase and chymase with ZN000008382327 inhibitor, a radius of gyration (Rg) was calculated and shown in Fig.5. The Rg value suggested that the binding of ZN000008382327 with chymase induced major structural changes and affected the structure and dynamics of chymase. The initial con-

Table 2. List of identified compounds and their ADMET properties

S. No.	Compound ID	Water solubility	BBB permeation	CYP2D6 Inhibitor	Toxicity skin sensitivity	GI absorption
1	ZN000003848531	Poorly soluble	No	No	-5.47 cm/s	Low
2	ZN000008382327	Poorly soluble	No	No	-6.90 cm/s	Low
3	N70	Poorly soluble	No	No	-6.33 cm/s	Low

Table 3. List of identified chymase inhibitors with their biological properties calculated through PASS web server (Lagunin *et al.*, 2000)

S. No	Compound ID	Pa	Pi	Biological activity
1	ZN000003848531	0,547	0,006	Glycine-tRNA ligase inhibitor
		0,325	0,084	Anti-infective
		0,289	0,064	Antibacterial
		0,629	0,010	Alcohol O-acetyltransferase inhibitor
3	ZN000008382327	0,799	0,013	G-protein-coupled receptor kinase inhibitor
		0,799	0,013	Beta-adrenergic receptor kinase inhibitor
		0,667	0,012	Antifungal
		0,592	0,013	Lactase inhibitor
4	N70	0,755	0,001	Chymase inhibitor
		0,753	0,005	Antihypertensive
		0,840	0,004	Antidiabetic
		0,431	0,031	Calcium regulator

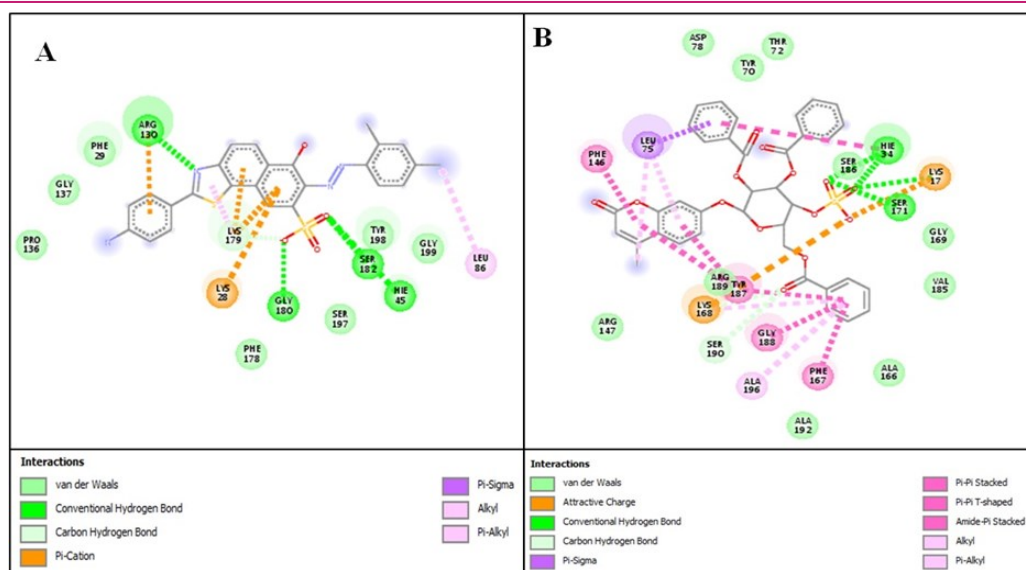


Fig. 2. Showing the two-dimensional interactions of chymase residues with inhibitors, A) Showing the interactions of chymase residues with ZN000008382327 inhibitor; B) Showing the interactions of chymase residues with ZN000003848531 inhibitor

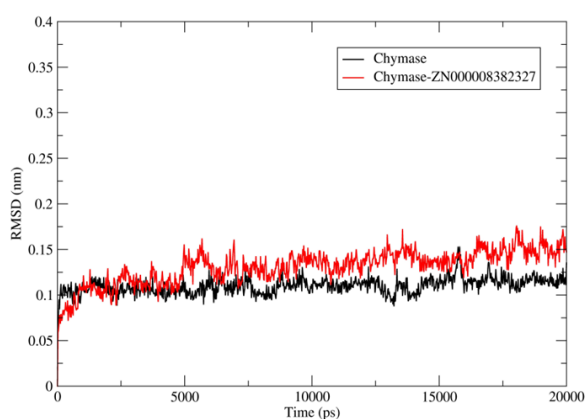


Fig. 3. RMSD of Ca backbone atoms of chymase protein. Chymase protein (black colour) showing less value of RMS compared to chymase with inhibitor ZN000008382327 complex (red)

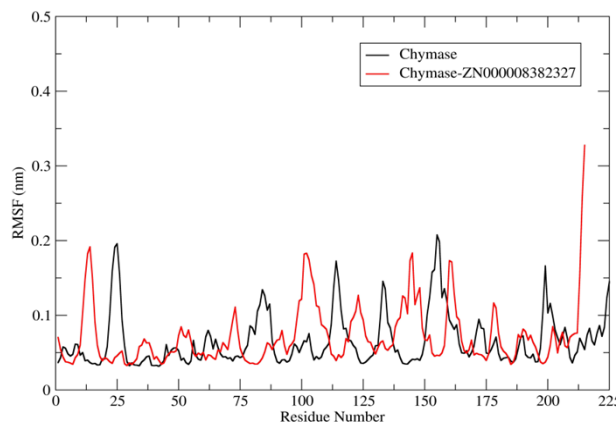


Fig. 4. Root mean square fluctuations of Ca backbone atoms of mast chymase (Colour codes are similar to Fig. for chymase with and without inhibitors)

Table 4. Hydrogen bonding interactions of chymase with inhibitors after molecular docking

Complex	Binding energy kcal/mol	Atoms involved in bonding	Bond distance Å	Bond angle	Fig. Ref
Chymase-ZN000003848531	-9.4	Gly180-NH...O-Drug	3.4	109.4	
		Tyr198-O...HC-Drug	2.8	120.9	
		Ser182-O...HO-Drug	2.1	118.7	
Chymase-ZN000008382327	-10.0	His45-N...HO-Drug	2.6	140.1	
		Lys28-HN...O-Drug	2.5	105.6	
		Gly199-NH...O-Drug	3.0	154.4	
		Ser201-CH...O-Drug	2.7	153.4	

formational fluctuations (up to 7ns) occur in the ZN000008382327 bound state chymase. After that, the complex is stable and equilibrated throughout the MD simulation suggesting the chymase-ZN000008382327 complex stability shown in Fig.5. Next, the solvent-accessible surface area values for free form of chymase and chymase with ZN000008382327 complex

were found to be 115 nm², respectively. Here, both systems showed a similar pattern of equilibration (Fig.6). The Rg and SASA plot showed the chymase protein's structural compactness and stability with the bound state of ZN000008382327 inhibitor.

The previous research work emphasized as to how the biological systems appear to be a potential in nature,

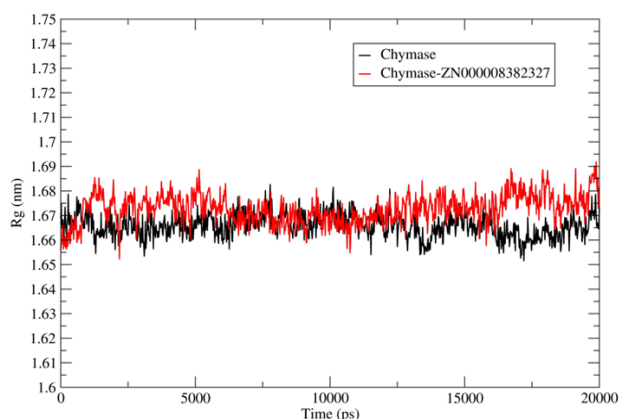


Fig. 5. Radius of gyration of mast chymase protein (Colour codes are similar to Fig. 3-4 for chymase with and without inhibitors)

concerning their molecular motions even at the atomic level. It is very much crucial to understand their enormous dynamic actions mainly due to the intercalation of therapeutic drugs into DNA, microtubules assemblages, switching occurs amongst both active and inactive states. The detailed investigation associated to internal motions has been reported (Wang and Chou, 2009, Chou *et al.*, 1994, Chou and Mao, 2004). The present work is very much aligned with these reports. However, the present study has conducted precise work on the potential behaviour of human chymase inhibitors using molecular docking and molecular dynamics simulation. Another report (Kushwaha *et al.*, 2021) investigated Molecular modeling inhibition in human chymase and its application. They proposed that Chymase-C3 is considered the least active chymase inhibitor in various investigations and which is generally saturated analogue of C2. Modifying one of the double bonds between two carbon atoms related to the C2 inhibitor to a single bond within C3 would bring significant change in its ability, which will help make it 180-folds less potent in comparison with the C2. They have also analyzed the C3 binding form which is slightly different concerning its structure, that had an immense effect on its binding conformation within the active site of the compact enzyme.

Recently there are two different erratic regulated experiments on *A. indica* capsule/extracts tested against Covid-19 patients and potentially recognized as promising natural remedies for treating SARS-CoV-2 (Khan *et al.*, 2020, Nesari *et al.*, 2021) RdRp and M^{pro} binding ability (Mpiana *et al.*, 2020; Abouelela *et al.*, 2021; Balkrishna *et al.*, 2021). The above studies have taken fewer compounds or related to only *Aloe vera*-specific phytochemicals for their investigation. The present study is not into the treatment; perhaps it will provide valuable insights for future drug designing and modelling.

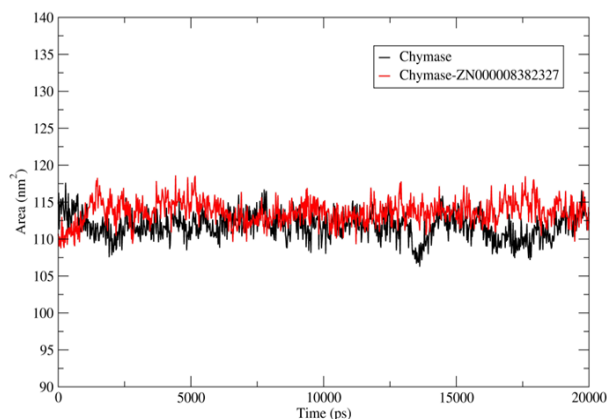


Fig. 6. Solvent accessible surface area of mast chymase protein (Colour codes are similar to Fig 3-4 for chymase with and without inhibitors)

Conclusion

The present investigation on the potential human chymase inhibitor using high throughput screening, ADMET, molecular docking, and complex stability using molecular dynamics simulations revealed two potential inhibitors based on ADMET property such as the compounds ZN000003848531 and ZN000008382327. Molecular docking confirmed the binding mode of ZN000003848531 and ZN000008382327 with chymase protein. The RMSD, RMSF, Rg, and SASA analysis showed that the ZN000008382327 inhibitor potentially affected the structure and dynamics of chymase protein and may be further used for experimental validation as well as for to design and development of new potential chymase inhibitors. One of the interesting features of the present work is that it will serve all necessary information about the human chymase inhibitors, and the inhibition of the chymase gene will probably trigger a new way of therapeutics for the treatment of allergic inflammation and cardiac disease.

Conflict of interest

The authors declare that they have no conflict of interest.

REFERENCES

1. Abouelela, M. E., Assaf, H. K., Abdelhamid, R. A., Elkhyat, E. S., Sayed, A. M., Oszako, T., *et al.* (2021). Identification of Potential SARS-CoV-2 Main Protease and Spike Protein Inhibitors from the Genus Aloe: An in silico Study for Drug Development. *Molecules.*, 26, 1–29.
2. Arooj, M., Kim, S., Sakkiah, S., Cao, P.G., Lee, Y. & Lee W.K. (2013). Molecular Modeling Study for Inhibition Mechanism of Human Chymase and Its Application in Inhibitor Design. *PLoS One.*, 8(4), e62740.
3. Balkrishna, A., Pokhrel, S., Singh, H., Joshi, M., Mulay, V. P., Haldar, S., *et al.* (2021). Withanone from *Withania Somnifera* Attenuates SARS-CoV-2 RBD and Host ACE2

- Interactions to Rescue Spike Protein Induced Pathologies in Humanized Zebrafish Model. *Drug Des. Devel. Ther.*, 15, 1111–1133.
4. Barret, R.N.(2018). Lipinski's rule of five. *Therapeutic Chemistry*, 1(1), 7-100.
 5. Biovia, D.S.(2015).Discovery Studio Modeling Environment. San Diego, Dassault Syst. Release, San Diego, 4.
 6. Case, D.A., Cheatham, T., Darden, T., Gohlke, H., Luo, R., Merz, K.M., Onufriev, C., Simmerling, B. & Woods, R. (2005). The amber biomolecular simulation programs. *J. Computat.Chem.*, 26, 1668-1688.
 7. Caughey, G.H. (2016). Mast cell proteases as pharmacological targets. *Eur J Pharmacol.*, 778, 44-55.
 8. Chou, K.C. & Mao, B. (2004). Collective motion in DNA and its role in drug intercalation. *Biopolymers.*, 27: 1795–1815.
 9. Chou, K.C., Zhang, C.T. & Maggiora, G.M. (1994). Solitary wave dynamics as a mechanism for explaining the internal motion during microtubule growth. *Biopolymers.*, 34: 143–153.
 10. Daina, A., Michielin, O. & Zoete, V. (2017). SwissADME: A free web tool to evaluate pharmacokinetics, drug-likeness and medicinal chemistry friendliness of small molecules. *Sci Rep.*, 7, 42717.
 11. DeLano, W.L. (2002). The PyMOL Molecular Graphics System. Delano Scientific, San Carlos.
 12. Doggrell, S.A. & Wanstall, J.C. (2004). Vascular chymase: Pathophysiological role and therapeutic potential of inhibition. *Cardiovasc. Res.*, 61(4), 653-62.
 13. Humphrey, W., Dalke, A. & Schulten, K.(1996).VMD: Visual molecular dynamics. *J Mol Graph.*, 14(1), 33-38.
 14. Kervinen, J., Crysler, C., Bayoumy, S., Abad, C.M., Spurlino, J., Deckman, I., Greco, N.M., Maryanoff, E.B. & Garavilla, D.W. (2010). Potency variation of small-molecule chymase inhibitors across species. *Biochem Pharmacol.*, 80(7), 1033-41.
 15. Khan, F. R., Kazmi, S. M. R., Iqbal, N. T., Iqbal, J., Ali, S. T. & Abbas, S. A. (2020). A Quadruple Blind, Randomised Controlled Trial of Gargling Agents in Reducing Intraoral Viral Load Among Hospitalised COVID-19 Patients: A Structured Summary of a Study Protocol for a Randomised Controlled Trial. *Trials* 21, 1–4.
 16. Kumbhar, B.V. & Bhandare, V.V. (2021). Exploring the interaction of Peloruside-A with drdrug-resistant β II and α III tubulin isotypes in human ovarian carcinoma using a molecular modeling approach. *J Biomol Struct Dyn.*, 39 (6), 1990-2002.
 17. Kumbhar, B.V., Bhandare, V.V., Panda, D. & Kunwar, A. (2020). Delineating the interaction of combretastatin A-4 with α β tubulin isotypes present in drug resistant human lung carcinoma using a molecular modeling approach. *J Biomol Struct Dyn.*, 38(2), 426-438.
 18. Kumbhar, B.V., Borogaon, A., Panda, D. & Kunwar, A. (2016). Exploring the origin of differential binding affinities of human tubulin isotypes α II, α III and α IV for DAMA-colchicine using homology modelling, molecular docking and molecular dynamics simulations. *PLoS One.*, 11(5), e0156048.
 19. Kushwaha, P.P., Singh, A.K., Bansal, T., et al. (2021). Identification of Natural Inhibitors Against SARS-CoV-2 Drugable Targets Using Molecular Docking, Molecular Dynamics Simulation, and MM-PBSA Approach. *Front Cell Infect Microbiol.*, 11:730288.
 20. Lagunin, A., Stepanchikova, A., Filimonov, D. & Poroikov, V. (2000). PASS: Prediction of activity spectra for biologically active substances. *Bioinformatics.*, 16(8), 747-748.
 21. Leskinen, M.J., Lindstedt, K.A., Wang, Y. & Kovanen, P.T. (2003). Mast cell chymase induces smooth muscle cell apoptosis by a mechanism involving fibronectin degradation and disruption of focal adhesions. *Arterioscler Thromb Vasc Biol.*, 23(2), 238-43.
 22. Lundequist, A., Abrink, M. & Pejler, G. (2006). Mast cell-dependent activation of pro matrix metalloprotease 2: A role for serglycin proteoglycan-dependent mast cell proteases. *Biological Chemistry.*, 387 (10-11), 1513-1519.
 23. Miyazaki, M., Takai, S. (2001). Local angiotensin II-generating system in vascular tissues: The roles of chymase. *Hypertens. Res.*, 24(3), 189-93.
 24. Morris, G.M., Ruth, H., Lindstrom, W., Sanner, F.M., Bellew, K.R., Goodsell, S.D. & Olson, J.A. (2009). Software news and updates AutoDock4 and AutoDockTools4: Automated docking with selective receptor flexibility. *J Comput Chem.*, 30, 2785-2791.
 25. Mpiana, P. T., Tshibangu, D. S., Kilembe, J. T., Gbolo, B. Z., Mwanangombo, D. T., Inkoto, C. L., et al. (2020). Aloe Vera (L.) Burm. F. As a Potential Anti-COVID-19 Plant: A Mini-Review of Its Antiviral Activity. *Eur. J. Med. Plants.*, 31, 86–93.
 26. Nesari, T. M., Bhardwaj, A., ShriKrishna, R., Ruknuddin, G., Ghildiyal, S., Das, A., et al. (2021). Neem (*Azadirachta Indica A. Juss*) Capsules for Prophylaxis of COVID-19 Infection: A Pilot, Double-Blind, Randomized Controlled Trial. *Altern. Ther. Health Med.*, 23, 1–8.
 27. Pejler, G. (2020). Novel Insight into the in vivo Function of Mast Cell Chymase: Lessons from Knockouts and Inhibitors. *J. Innate Immun.*, 12(5), 357-372.
 28. Roszkowska-Chojecka, M.M., Walkowska, A., Gawrys, O., Baranowska, I., Kalisz, M., Litwiniuk, A., Martynska, L. & Jezierska, K.E. (2015). Effects of chymostatin, a chymase inhibitor, on blood pressure, plasma and tissue angiotensin II, renal haemodynamics and renal excretion in two models of hypertension in the rat. *Exp Physiol.*, 100 (9),1093-105.
 29. Sterling, T. & Irwin, J.J. (2015). ZINC15 Ligand Discovery for Everyone. *J Chem Inf Model.*, 55(11), 2324-37.
 30. Takai, S. & Jin, D., Sakaguchi, M., Katayama, S., Muramatsu, M., Sakaguchi, M., Matsumura, E., Kim, S., Miyazaki, M. (2003). A novel chymase inhibitor, 4-[1-[[bis-(4-methyl-phenyl)-methyl]-carbonyl]-3- (2-ethoxy-benzyl)-4-oxo-azetidine-2-yloxy]-benzoic acid (BCEAB), suppressed cardiac fibrosis in cardiomyopathic hamsters. *J Pharmacol Exp Ther.*, 305(1), 17-23.
 31. Tani, M., Harimaya, K., Gyobu, Y., Sasaki, T., Takenouchi, O., Kawamura, T., Kamimura, T. & Harada, T.(2004). SF2809 compounds, novel chymase inhibitors from *Dactylosporangium sp. 1*. Taxonomy, fermentatation, isolation and biological properties. *J Antibiot (Tokyo).*, 57(2), 83-8.
 32. Tchougounova, E., Lundequist, A., Fajardo, I., Winberg, J., Abrink, M. & Pejler, G. (2005). A key role for mast cell chymase in the activation of pro-matrix metalloprotease-9 and pro-matrix metalloprotease-2. *J Biol Chem.*, 280(10), 9291-9296.
 33. Tomimori, Y., Manno, A., Tanaka, T., Takahashi, F.J., Muto, T., Nagahira, K. (2019). ASB17061, a novel chy-

- mase inhibitor, prevented the development of angiotensin II-induced abdominal aortic aneurysm in apolipoprotein E-deficient mice. *Eur J Pharmacol.*, 5, 856, 172403.
34. Trott, O. & Olson, A.J. (2010). AutoDock Vina: Improving the speed and accuracy of docking with a new scoring function, efficient optimization, and multithreading. *J Comput Chem.*, 31(2), 455-461.
35. Turner, P.J. (2005). XMGRACE, Version 5.1.19. Center for Coastal and Land-Margin Research, Oregon Graduate Institute of Science and Technology, Beaverton.
36. VanDer, S.D., Lindahl, E., Hess, B., Groenhof, G., Mark, E.A. & Berendsen, J.C.H. (2005). GROMACS: Fast, flexible, and free. *J. Comput. Chem.*, 26, 1701-1718.
37. Wang, J.F. & Chou, K.C. (2009). Insight into the molecular switch mechanism of human Rab5a from molecular dynamics simulations. *Biochemical and Biophysical Research Communications*, 390, 608–612.
38. Warnecke, A., Sandalova, T., Achour, A. & Harris, R.A. (2014). PyTMs: a useful PyMOL plugin for modeling common post-translational modifications. *BMC Bioinformatics.*, 15, 370.
39. Zhang, M., Huang, W., Bai, J., Nie, X. & Wang, W. (2016). Chymase inhibition protects diabetic rats from renal lesions. *Mol Med Rep.*, 14(1), 121-8.